SYMBOL INTERFERENCE

Digitally modulated signals convey information with symbols that are sequentially transmitted during periodic time intervals or symbol periods. The symbols may represent one or more bits of digital information. Intersymbol interference (ISI) occurs when extraneous energy from one symbol period interferes with energy in a different symbol period. Intersymbol interference is caused by band-limiting filters in the transmitter and receiver, channel filtering due to the propagation medium that lies between the transmitter and receiver, and symbol sample timing errors. Intersymbol interference is detrimental because it causes the error ratio of a digital communications radio link to increase. The error ratio is the number of bits or symbols received in error divided by the total number of bits or symbols transmitted.

Figure 1 is a block diagram of a digital communications radio link operating at a carrier frequency. The symbols to be transmitted scale the amplitude of a train of wideband pulses that are spaced T seconds apart. The pulse shape filter bandlimits the symbols and can introduce ISI if not carefully de-

J. Webster (ed.), *Wiley Encyclopedia of Electrical and Electronics Engineering*. Copyright © 1999 John Wiley & Sons, Inc.

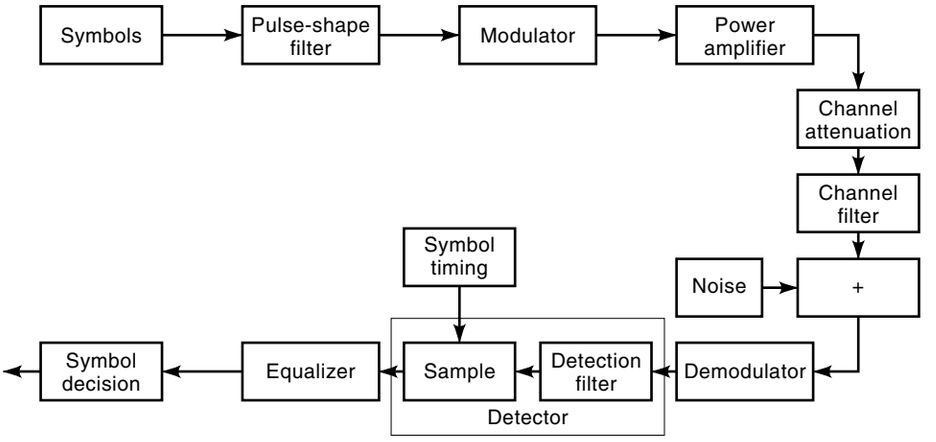

Figure 1. Block diagram of digital communication radio link showing the location of filters that sometimes introduce ISI.

signed. The band-limited symbols then modulate the carrier amplitude, phase, frequency, or some combination of these. The modulated carrier is power-amplified and transmitted through the channel. The channel attenuates and, in some instances, filters the modulated carrier. Channel filtering introduces ISI; however, channel attenuation does not.

The demodulator converts the modulated carrier back to band-limited symbols. The detector filters the signal to minimize noise power and samples the signal once per symbol period. The detector filter can introduce ISI if not properly designed. Equalization attempts to remove ISI from the samples prior to the decision operation. In parallel with these receiver operations are other important tasks, such as symbol timing estimation, which can also introduce ISI.

Signal distortion caused by imperfect modulation, power amplification, demodulation, and carrier recovery can also cause ISI; however, these effects are not discussed in this article. Although additive noise and interference do not cause ISI directly, they may contribute to ISI by adding uncertainty to symbol sample timing estimation.

For radio applications, band-limiting ISI can be eliminated or minimized through proper design of the transmitter and receiver filters; however, channel filtering is often unavoidable due to the characteristics of the propagation medium (i.e., ionosphere, troposphere, or urban environment). For this reason, prevention of band-limiting ISI using Nyquist's criteria for signal design (1) will be discussed before examples of band-limiting filters are presented while mitigation of channel filtering will be discussed after methods of classifying, modeling, and measuring the channel filter have been presented. Finally, quantification of the effect of ISI on a digital communications radio link is discussed—that is, the degradation of the error ratio for various combinations of band-limiting filters, channel filters, and symbol sample timing conditions.

BAND-LIMITING

Band-limiting is introduced by filters in the transmitter and receiver. These filters may produce demodulated symbols with ISI if they are not carefully designed. Nyquist proposed three ISI criteria for band-limiting filters that eliminate ISI at the symbol sample time, between symbol sample times, and during the symbol period (2). He also proposed two ISI theorems that allowed engineers to design practical filters using the ISI criteria. These ISI criteria and theorems are used today to design filters for many radio applications (3). In this section, Nyquist's ISI criteria and theorems are presented, and commonly used band-limiting filters are discussed in terms of the criteria.

Prevention of Band-Limiting Intersymbol Interference

Nyquist's first ISI criterion states that ISI at the symbol sample time, kT, can be eliminated in band-limited signals if the filter impulse response satisfies

$$y(kT) = \begin{cases} 1, & k = 0 \\ 0, & k \neq 0 \end{cases} \tag{1}$$

The ideal low-pass filter meets this criterion. The transfer function of an ideal low-pass filter is

$$Y(f) = \begin{cases} T, & |f| \leq f_c \\ 0, & |f| > f_c \end{cases} \tag{2}$$

where f_c represents the ideal low-pass filter cutoff frequency, referred to as the Nyquist frequency, and $f_c = 1/(2T)$. The ideal low-pass filter impulse response is

$$y(t) = \text{sinc}(t/T) \tag{3}$$

where $\text{sinc}(x) \equiv \sin(\pi x)/\pi x$. Nyquist's first criterion is perhaps the most commonly cited of the three criteria because it addresses ISI at the symbol sample time.

Nyquist's second ISI criterion states that ISI at the transition time half-way between symbols, $kT + T/2$, can be eliminated in band-limited signals if the filter impulse response satisfies

$$y(kT + T/2) = \begin{cases} \frac{1}{2}, & k = 0, -1 \\ 0, & k \neq 0, -1 \end{cases} \tag{4}$$

The cosine filter meets this criterion. The cosine filter transfer function is

$$Y(f) = \begin{cases} T\cos\dfrac{\pi f}{2f_c}, & |f| \le f_c \\ 0, & |f| > f_c \end{cases} \tag{5}$$

The cosine filter impulse response is

$$y(t) = \frac{2\cos(\pi t/T)}{\pi(1-4t^2/T^2)} \tag{6}$$

The output at the transition time will be proportional to the sum of the values at kT and $(kT + T)$. This result indicates that signal zero crossings, useful for symbol timing estimation, can be ISI-free at the transition times. In addition, this result shows that differential detection can be accomplished without ISI.

Nyquist's third ISI criterion states that ISI in the symbol period can be eliminated in band-limited signals if the impulse response satisfies

$$\int_{-T/2}^{T/2} y(t-kT)\,dt = \begin{cases} 1, & k = 0 \\ 0, & k \ne 0 \end{cases} \tag{7}$$

The reciprocal sinc filter meets this criterion. The reciprocal sinc filter transfer function is

$$Y(f) = \begin{cases} T\,\mathrm{sinc}^{-1}\left(\dfrac{f}{2f_c}\right), & |f| \le f_c \\ 0, & |f| > f_c \end{cases} \tag{8}$$

The third criterion is used to eliminate ISI in constant-envelope modulations such as tamed-frequency modulation where time-varying frequencies are integrated over a symbol period to represent discrete phase values (4). The third criterion is closely related to Nyquist's first criterion. Indeed

$$Y_3(f) = Y_1(f)\mathrm{sinc}^{-1}\left(\frac{f}{2f_c}\right) \tag{9}$$

where $Y_1(f)$ and $Y_3(f)$ refer to filter transfer functions that meet Nyquist's first and third criterion, respectively (5).

The vestigial symmetry theorem extends these results beyond the ideal low-pass filter and cosine filter described previously in the first and second criterion. This extension is useful because it allows the designer to construct filters that meet the criteria with impulse responses that have desirable qualities such as causality, faster decay times, and broader central peaks. Faster decay times decrease ISI in practical systems by decreasing the contributions of past symbols while broader central peaks relax specifications on symbol sample timing. The vestigial symmetry theorem does not apply directly to the third criterion.

Vestigial symmetry, in this context, refers to symmetry about f_c. The vestigial symmetry theorem states that the sum of a vestigially symmetric transfer function and a transfer function that meets the first or second criterion will also meet the criterion. The type of vestigial symmetry differs for each criterion. Vestigial symmetry for the first criterion is

$$V(f_c - f) = -V^*(f_c + f), \qquad |f| \le f_c \tag{10}$$

where * denotes conjugation, Re$\{V(f)\}$ has odd vestigial symmetry, and Im$\{V(f)\}$ has even vestigial symmetry. Other transfer functions that meet the first criterion, beyond the ideal low-pass filter, can be derived using

$$Y(f) = \begin{cases} T + V(f), & |f| \le f_c \\ V(f), & |f| > f_c \end{cases} \tag{11}$$

Vestigial symmetry for the second criterion is

$$V(f_c - f) = V^*(f_c + f), \qquad |f| \le f_c \tag{12}$$

where Re$\{V(f)\}$ has even vestigial symmetry and Im$\{V(f)\}$ has odd vestigial symmetry. Similarly, other transfer functions that meet the second criterion, beyond the cosine filter, can be derived using

$$Y(f) = \begin{cases} T\cos\left(\dfrac{\pi f}{2f_c}\right) + V(f), & |f| \le f_c \\ V(f) & |f| > f_c \end{cases} \tag{13}$$

Nyquist also formulated a generalized pulse-shape theorem. This theorem is important because it allows a transfer function meeting any of Nyquist's criterion to be distributed across more than one filter. The generalized pulse-shape theorem states that pulses that do not meet a criterion can be modified to meet the criterion by the addition of a network with the transfer function

$$Y_S(f) = \frac{Y(f)}{S(f)} \tag{14}$$

where $Y(f)$ is the transfer function that meets a criterion and $S(f)$ is the transfer function that does not meet a criterion. This theorem is used in designing equalizers for channel filters and distributing the transfer function of a filter that meets a criterion across the pulse-shape filter and detector filter.

Band-Limiting Filter Types

The full raised cosine filter satisfies the first and second criteria; thus, the full raised cosine filter eliminates ISI at symbol sample times and transition times. The major disadvantage of the full raised cosine filter is that it takes twice as much bandwidth as the ideal low-pass filter. The full raised cosine filter can be built from either the first or second criterion using appropriate vestigially symmetric transfer functions. When

$$V(f) = \begin{cases} \dfrac{T}{2}\left(-1 + \cos\left(\dfrac{\pi f}{2f_c}\right)\right), & |f| \le f_c \\ \dfrac{T}{2}\left(1 + \cos\left(\dfrac{\pi f}{2f_c}\right)\right), & f_c < |f| \le 2f_c \end{cases} \tag{15}$$

is added to the ideal low-pass filter transfer function or when

$$V(f) = \begin{cases} \dfrac{T}{2}\left(1 - \cos\left(\dfrac{\pi f}{2f_c}\right)\right), & |f| \le f_c \\ \dfrac{T}{2}\left(1 + \cos\left(\dfrac{\pi f}{2f_c}\right)\right), & f_c < |f| \le 2f_c \end{cases} \tag{16}$$

is added to the cosine filter transfer function, the full raised cosine filter transfer function is produced:

$$Y(f) = \begin{cases} \frac{T}{2}\left(1 + \cos\left(\frac{\pi f}{2f_c}\right)\right), & |f| \le 2f_c \\ 0, & |f| > 2f_c \end{cases} \tag{17}$$

The full raised cosine filter impulse response is

$$y(t) = \text{sinc}\left(\frac{t}{T}\right)\frac{\cos(\pi t/T)}{1 - 4t^2/T^2} \tag{18}$$

The raised cosine filter is used more commonly than the full raised cosine filter. The raised cosine filter satisfies the first criterion; however, it does not satisfy the second criterion and therefore has ISI at the transition times. The raised cosine filter one-sided bandwidth is $f_c + \alpha f_c$, where α is the excess bandwidth coefficient that ranges from 0 to 1. Zero represents the ideal low-pass filter while 1 represents the full raised cosine filter. The transfer function of the raised cosine filter is

$$Y(f) = \begin{cases} T, & |f| \le f_c - \alpha f_c \\ \frac{T}{2}\left(1 + \cos\left(\frac{\pi(|f| - (f_c - \alpha f_c))}{2\alpha f_c}\right)\right), & f_c - \alpha f_c < |f| \le f_c + \alpha f_c \\ 0, & f_c + \alpha f_c < |f| \end{cases} \tag{19}$$

The corresponding impulse response of the raised cosine filter is

$$y(t) = \text{sinc}\left(\frac{t}{T}\right)\frac{\cos(\pi\alpha t/T)}{1 - 4\alpha^2 t^2/T^2} \tag{20}$$

The raised cosine filter eliminates ISI at the symbol sample time only if symbol sample timing recovery is perfect. The double-jump (DJ) filter satisfies Nyquist's first criterion while minimizing the mean-squared error (MSE) between the transmitted and received signals when timing error is introduced by the receiver (6,7). The DJ filter has an excess bandwidth αf_c like the raised cosine filter. This filter is referred to as the double-jump filter because its transfer function has two steep transitions or "jumps" at $f_c - \alpha f_c$ and $f_c + \alpha f_c$. The transfer function of the DJ filter that minimizes the MSE with timing recovery error is

$$Y(f) = \begin{cases} T, & |f| & \le f_c - \alpha f_c \\ \frac{T}{2}\left(2 - \frac{|f|}{f_c}\right), & f_c - \alpha f_c < |f| & \le f_c + \alpha f_c \\ 0, & f_c + \alpha f_c < |f| & \end{cases} \tag{21}$$

It is not always possible or advantageous to use band-limiting filters that satisfy Nyquist's criteria. In portable radio applications, for example, the ISI resulting from channel filtering may be much greater than the ISI resulting from band-limiting. For this reason, the effect that suboptimum pulse-shape filtering and detection filtering has on error ratio has been analyzed. For example, researchers have investigated the signal-to-noise (SNR) degradation of phase shift-keying modulation caused by using a Chebyshev pulse-shaping filter with a Butterworth detection filter (8). An SNR degradation of approximately 1 dB was found when the Chebyshev pulse-shaping filter had a time-bandwidth product, BT, of 2.0 and the Butterworth detection filter had a BT of 1.0.

Portable radio designers frequently use constant-envelope modulations with pulses that do not satisfy Nyquist's third criterion. Gaussian minimum shift keying (GMSK) modulation, for example, uses a Gaussian pulse-shape filter. Researchers have found that the SNR degradation of GMSK is less than 1 dB for Gaussian filters with a BT greater than 0.5 (9).

Partial response pulse-shape filters do not satisfy any of Nyquist's criteria; instead, they introduce ISI intentionally. However, since the amount of ISI introduced is known, the ISI can be removed by the receiver. The duobinary partial response filter (10) has a transfer function

$$Y(f) = \begin{cases} T(1 + e^{-j\pi|f|/f_c}), & |f| \le f_c \\ 0, & |f| > f_c \end{cases} \tag{22}$$

and a corresponding impulse response

$$y(t) = \text{sinc}\left(\frac{t}{T}\right) + \text{sinc}\left(\frac{t - T}{T}\right) \tag{23}$$

Measurement of Band-Limiting Intersymbol Interference

Band-limiting ISI can be viewed with constellation, vector, and eye diagrams (11,12). The eye diagram is a visual display of the time-varying amplitude of the demodulated signal after the in-phase (I) or quadrature-phase (Q) detection filter. The eye diagram displays several demodulated signal segments, NT seconds in duration, on the same graph. The amplitude at the symbol sample time and the time delay of the zero crossings from the transition times are commonly measured eye diagram parameters. Statistics of these, such as their peak, mean, standard deviation, and minimum, are used to predict performance degradation of digital communication radio links.

The vector diagram shows the time-varying amplitude and phase of the demodulated signal after the detection filters on an I/Q graph. The constellation diagram simplifies the vector diagram by showing the amplitude and phase at symbol sample times only. Statistics of the vector diagram error vector or constellation diagram error vector, resulting from subtracting the measured diagram from an undistorted diagram, are reported. Figures 2 and 3 show a digitally demodulated signal without and with ISI, respectively, with all three diagrams.

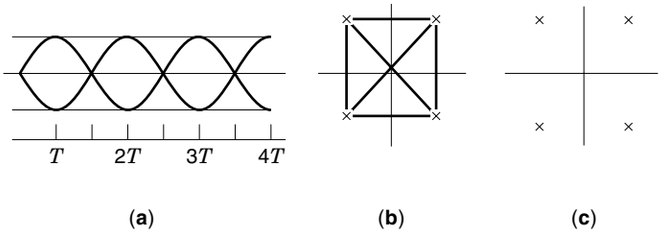

Figure 2. Eye diagram (a), vector diagram (b), and constellation diagram (c) of signal without ISI at the symbol sample times and transition times.

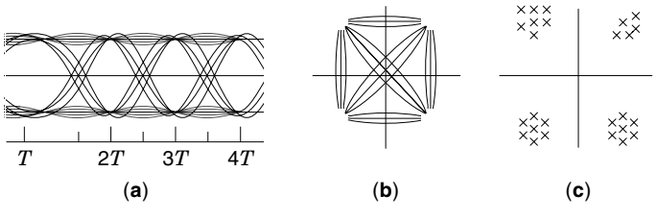

Figure 3. Eye diagram (a), vector diagram (b), and constellation diagram (c) of signal with ISI at symbol sample times and transition times.

CHANNEL FILTERING

Intersymbol interference can also be caused by the channel filter. In this section, channel filtering will be assumed to be due to the propagation of an unguided wave through a radio channel such as the ionosphere, troposphere, or urban environment; however, in practice, waves propagated through a waveguide or transmission line can also be channel-filtered (13,14). Mitigation of channel filtering with techniques such as equalization is discussed after a description of channel filter types, measurements, and models.

Channel Filter Types

Radio channel filtering is predominately caused by multipath. The effect that multipath has on the transmitted signal is dependent upon the signal bandwidth. The multipath is considered frequency-nonselective if the transfer function amplitude and group delay are constant over frequencies in the transmitted signal bandwidth. The frequency-nonselective multipath channel degrades the radio link by attenuating the signal; however, it does not introduce ISI. The multipath is frequency-selective if the transfer function amplitude and group delay vary over the frequencies in the transmitted signal bandwidth. The frequency-selective multipath channel degrades the radio link by introducing attenuation and ISI. Figure 4 shows the transfer function amplitude for frequency-nonselective and frequency-selective channels.

Two frequency-selective multipath channels are commonly analyzed: the specular multipath channel, composed of a small number of distinct paths with irregular time delays,

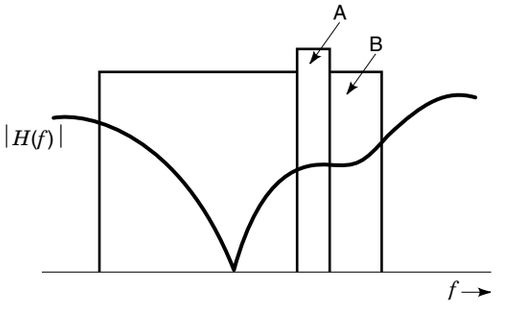

Figure 4. Curve representing the amplitude of the channel transfer function. Small rectangular box A represents the bandwidth of a signal subjected to frequency-nonselective multipath, and large rectangular box B represents bandwidth of a signal subjected to frequency-selective multipath. Frequency-selective multipath channels introduce ISI while frequency-nonselective multipath channels do not.

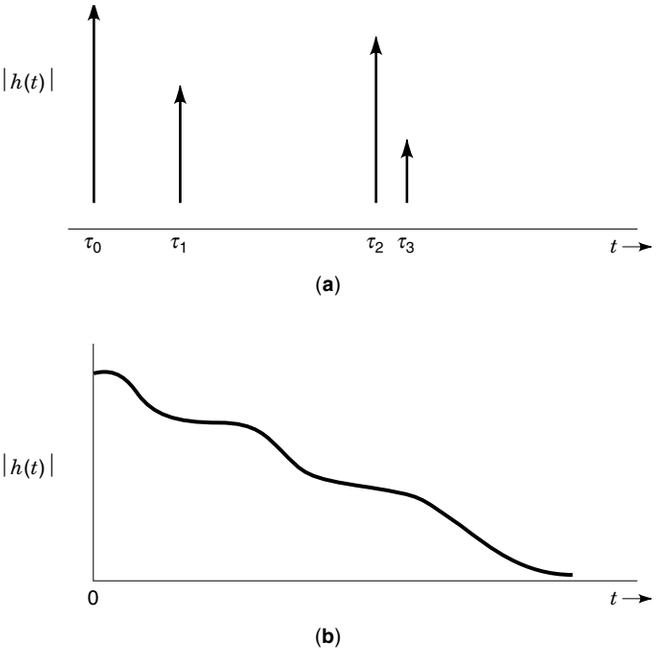

Figure 5. Impulse response magnitude of a specular (a) and diffuse (b) multipath channel. Specular multipath channels have irregularly spaced path time delays whereas diffuse multipath channels are a continuum of paths.

and the diffuse multipath channel, composed of a continuum of paths. Figure 5 shows the impulse response amplitude for diffuse and specular multipath channels.

The two-path, specular multipath channel is found in applications such as line-of-sight microwave radio (15). It is represented by the impulse response.

$$h(t) = \delta(t) + \beta\delta(t - \tau) \tag{24}$$

where β is the complex reflection coefficient and τ is the time delay of the reflected path. Its corresponding transfer function is

$$H(f) = 1 + \beta e^{-j2\pi f\tau} \tag{25}$$

The reflection coefficient is assumed to be constant over the transmitted signal bandwidth and have a magnitude less than 1. Figure 6 shows the impulse response and transfer function for arbitrary reflected path parameters. The reflected path time shift corresponds to the linear phase shift in the transfer function. The maxima and minima (nulls) in the transfer function repeat every $1/\tau$ Hz at frequencies of

$$\frac{\angle\beta \pm n\pi}{2\pi\tau} \tag{26}$$

The minima occur when n is odd, while the maxima occur when n is even. The magnitude of the maxima is

$$\sqrt{1 + 2|\beta| + |\beta|^2} \tag{27}$$

the magnitude of the minima is

$$\sqrt{1 - 2|\beta| + |\beta|^2} \tag{28}$$

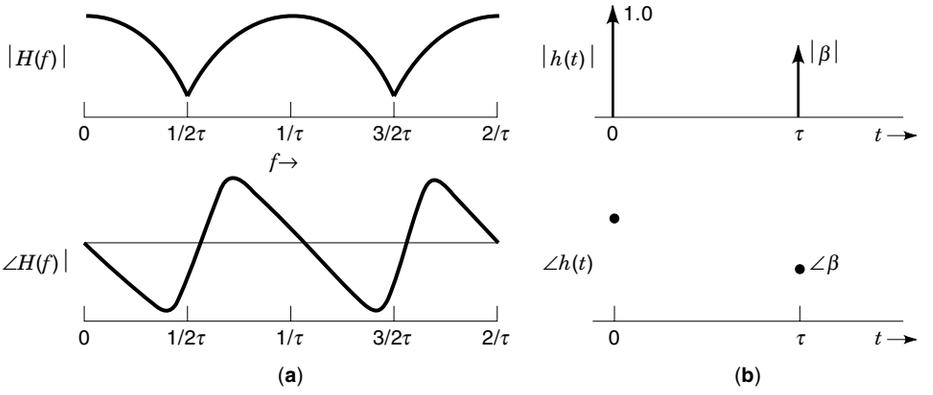

Figure 6. Complex transfer function (a) and complex impulse response (b) of a two-path, specular multipath channel. The amplitude of the transfer function shows nulls due to the existence of a second path.

and the phase passes through zero at the maxima and minima.

Diffuse multipath channels are found in ionospheric, troposcatter, and mobile radio applications. These channels are characterized by the power delay profile (PDP), $P_h(t)$, when the impulse response changes with starting time or position (16,17). The PDP is related to the autocorrelation of the wide-sense-stationary (WSS) channel transfer function

$$R_{\mathrm{H}}(f+\Omega, f) = E[H(f+\Omega)H^*(f)] \tag{29}$$

where $E[\ ]$ is the expected value and Ω is the frequency offset, by the Fourier transform

$$P_h(t) = \int_{-\infty}^{\infty} R_{\mathrm{H}}(f+\Omega, f)e^{j2\pi\Omega t}\,d\Omega \tag{30}$$

It can also be shown that the autocorrelation of the impulse response

$$R_{\mathrm{h}}(s,t) = E[h(s)h^*(t)] \tag{31}$$

is related to the PDP by

$$R_{\mathrm{h}}(s,t) = \delta(t-s)P_{\mathrm{h}}(s) \tag{32}$$

Thus, a diffuse multipath channel with a WSS transfer function has uncorrelated impulse responses. It is called a wide-sense-stationary, uncorrelated scattering (WSSUS) channel.

The Gaussian wide-sense stationary uncorrelated scattering (GWSSUS) channel is frequently used to represent diffuse multipath channels. The properties of the GWSSUS channel are identical to the WSSUS with the addition that the impulse response amplitudes are complex Gaussian distributed (18). The discrete representation of the GWSSUS channel is

$$h_k = N\left[0, \frac{\sigma_k^2}{2}\right] + jN\left[0, \frac{\sigma_k^2}{2}\right] \tag{33}$$

where $N[m, \sigma^2]$ represents a Gaussian random process with mean m and variance σ^2, and

$$\sigma_k^2 = P_h(k\Delta\tau) \tag{34}$$

where $\Delta\tau$ is the time-delay interval.

Channel Filter Measurement

The impulse response of a multipath channel is commonly measured with a wideband channel probe (19,20). The probe transmits a psuedorandom noise (PN) signal

$$z(t) = \sum_{k=0}^{\infty}\sum_{l=1}^{N_{\mathrm{c}}} a_l\, p(t - kN_{\mathrm{c}}T_{\mathrm{c}} - lT_{\mathrm{c}}) \tag{35}$$

where a_l is a PN "chip" value, $p(t)$ is the PN chip pulse-shape, N_{c} is the number of chips per PN "word," and T_{c} is the PN chip period, whose autocorrelation approximates a wideband pulse

$$x(t) = \frac{1}{N_{\mathrm{c}}T_{\mathrm{c}}}\int_{t_0-N_{\mathrm{c}}T_{\mathrm{c}}}^{t_0} z(s)z^*(s+t)\,ds \tag{36}$$

where t_0 is an arbitrary time.

The channel probe receives the signal

$$w(t) = z(t) * h(t) \tag{37}$$

where $h(t)$ is the impulse response. The multipath signals are correlated with z in the receiver using

$$y(t) = \frac{1}{N_{\mathrm{c}}T_{\mathrm{c}}}\int_{t_0-N_{\mathrm{c}}T_{\mathrm{c}}}^{t_0} z^*(\tau - t)w(\tau)\,d\tau \tag{38}$$

This can be shown to be equal to

$$y(t) = \int_{t_0-N_{\mathrm{c}}T_{\mathrm{c}}}^{t_0} x(t-\sigma)h(\sigma)\,d\sigma \tag{39}$$

which approximates $h(t)$ when $x(t)$ is a wideband pulse.

Two types of channel probe receivers, which differ in how the correlation is performed, are commonly used: sliding correlator (21) and digital (22). The sliding correlator receiver performs the correlation in the time domain with analog circuitry, whereas the digital receiver performs the correlation in the frequency domain using digital signal-processing algorithms.

A few precautions must be taken when measuring channel impulse responses. First, the maximum time delay range, $N_{\mathrm{c}}T_{\mathrm{c}}$, cannot be exceeded. Second, the time delay resolution of the channel probe is limited to T_{c}. Third, the bandwidth of

the transmitted PN chips, $1/T_c$, needs to be 5 to 10 times the application signal bandwidth so distortion by the channel probe is minimized. Fourth, the type of antenna used in the measurements should be similar to, if not identical to, the antennas used by the application.

The PDP can be estimated from the output autocorrelation of the channel impulse response measurement. If the output signal is

$$y(t) = x(t) * h(t) \tag{40}$$

then the output autocorrelation is

$$R_y(s,t) = E[y(s)y^*(t)] \tag{41}$$

Using the definition of $R_h(s, t)$, it can be shown that

$$R_y(s,t) = \int_{-\infty}^{+\infty} x(t-\tau)x^*(s-\tau)P_h(\tau)\,d\tau \tag{42}$$

and

$$R_y(t,t) = \int_{-\infty}^{+\infty} |x(t-\tau)|^2 P_h(\tau)\,d\tau \tag{43}$$

Therefore, if $x(t)$ is a wideband pulse the PDP can be approximated with the output autocorrelation. Using this result, the PDP is approximated with channel impulse response measurements obtained over an area or time period likely to yield a sufficient number of independent, statistically stationary impulse responses by

$$R_y(t,t) = \frac{1}{N}\sum_{n=1}^{N} |y(t,n)|^2 \tag{44}$$

where $y(t, n)$ represents the nth independent channel impulse response measurement. Figure 7 shows the PDP and impulse response magnitude of a measured channel.

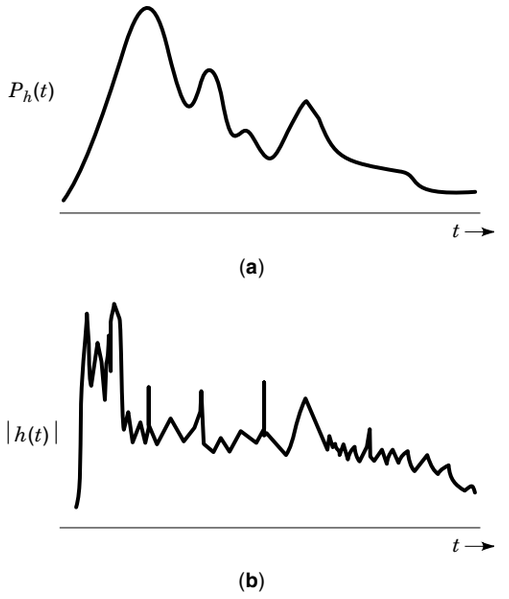

Figure 7. Measured power delay profile and impulse response amplitude of a WSSUS multipath channel. The PDP is smoother than the amplitude of the impulse response since it is the result of averaging several independent impulse response measurements.

Channel Filter Modeling

Several channel filter modeling methods have been shown to closely mimic channel filter measurements. For example, three methods using electromagnetic modeling principles—namely, geometric optics (or ray tracing) models (23,24), finite-difference time-domain (FDTD) models (25,26), and time-domain integral-equation models (27)—have been used to calculate the impulse response of a frequency-selective multipath channel. Models using these methods are advantageous because they can be applied to a number of different environments; however, they can require long computation times.

Statistical models have also been developed for the channel filter (28–30). Statistical models are computationally less demanding; however, they are derived from measurements, which can be time-consuming to acquire. A model utilizing acoustic resonance techniques has been developed that estimates indoor channel PDPs (26,31). The model assumes that the indoor room behaves like a "dead" acoustic cavity that significantly attenuates paths reflecting off the walls, floor, and ceiling in less than 10 reflections. The model is able to predict the PDP quickly for any arbitrary room dimension.

Mitigation of Channel Filter Intersymbol Interference

Channel filter effects are frequently mitigated with equalization. Prior to discussing equalization, a consistent mathematical nomenclature for the blocks depicted in Fig. 1 is established. The sequence of symbols to be transmitted is represented as a vector $I = \{i_0, i_1, \ldots, i_m\}$. The train of wideband pulses scaled by symbol values is

$$a(t) = \sum_{m=0}^{\infty} i_m \delta(t - mT) \tag{45}$$

where T is the symbol period, the band-limited symbol signal is

$$d(t) = \sum_{m=0}^{\infty} i_m p(t - mT) \tag{46}$$

where $p(t)$ is the pulse-shape filter impulse response, and the digitally modulated signal is

$$s(t) = \mathrm{MOD}[d(t)] \tag{47}$$

where MOD is the modulation operation (i.e., amplitude shift-keying, frequency shift-keying, or phase shift-keying). The signal at the output of the channel is represented as

$$r(t) = h(t) * s(t) \tag{48}$$

where $h(t)$ is the channel impulse response, the demodulated signal is

$$u(t) = \mathrm{DEM}[r(t)] \tag{49}$$

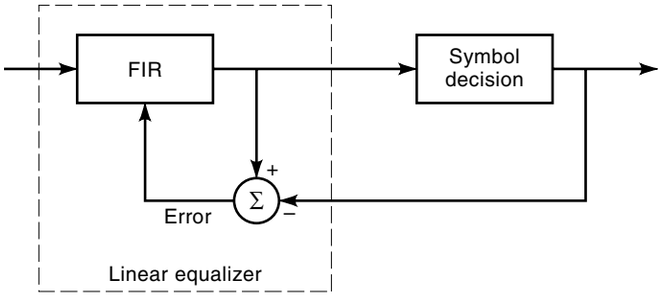

Figure 8. Block diagram of a linear equalizer used to mitigate channel filtering. The error signal is used to adjust the FIR filter tap weights.

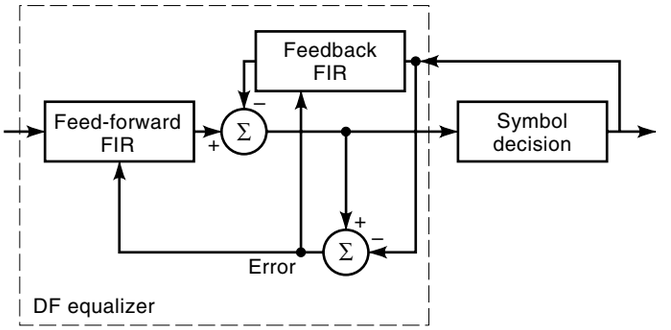

Figure 9. Block diagram of a decision feedback equalizer used to mitigate channel filtering. The error signal is used to adjust the feedforward FIR and feedback FIR filter tap weights.

where DEM is the demodulation operation, and the detection filtered signal is

$$v(t) = u(t) * g(t) \tag{50}$$

where $g(t)$ is the detection filter impulse response. Finally we represent the sampled signal as

$$V = \sum_{m=0}^{\infty} v(t - mT) \tag{51}$$

where $V = \{v_0, v_1, \ldots, v_m\}$, the equalized signal as

$$W = \text{EQU[V]} \tag{52}$$

where EQU is the equalizer function and $W = \{w_0, w_1, \ldots, w_m\}$, and the estimated symbols as

$$\hat{I} = \text{DEC}[W] \tag{53}$$

where DEC is the decision function and $\hat{I} = \{\hat{\imath}_0, \hat{\imath}_1, \ldots, \hat{\imath}_m\}$.

There are three common equalization methods: linear, decision feedback (DF), and maximum likelihood sequence estimation (MLSE) (32–34). The linear equalizer is composed of a finite impulse response filter (FIR) as shown in Fig. 8. The equalized signal is

$$w_k = \sum_{j=-K}^{K} c_j v_{k-j} \tag{54}$$

where c represents the FIR tap weights. The tap weight values are chosen to minimize the MSE between the transmitted and estimated symbols.

The DF equalizer is a nonlinear equalizer that subtracts previously estimated symbols from the sampled signal. The DF equalizer is composed of feedforward and feedback FIR filters as shown in Fig. 9. The equalized signal is

$$w_k = \sum_{j=-k}^{0} c_j v_{k-j} - \sum_{j=1}^{K} c_j \hat{\imath}_{k-j} \tag{55}$$

Like the linear equalizer, the equalizer tap weights are chosen to minimize the MSE between the transmitted and estimated symbols.

The MLSE equalizer works by minimizing the probability of error. Figure 10 shows a block diagram of a MLSE equalizer. The channel impulse response estimate, $\hat{h}$, is used to introduce ISI in the hypothetical transmitted symbol sequence $B = \{b_0, b_1, \ldots, b_m\}$:

$$c_k = \sum_{j=0}^{L-1} \hat{h}_j b_{k-j} \tag{56}$$

where L is the length of the ISI "trellis." The estimated symbol, $\hat{\imath}_{k-L+1}$, is the $k - L + 1$ symbol of B that minimizes

$$\sum_{j=0}^{L-1} |v_{k-l} - c_{k-l}|^2 \tag{57}$$

The channel impulse response estimate is also convolved with $\hat{I}$ to generate an error signal for channel impulse response estimation.

Each method has its distinct advantages and disadvantages. In general, the linear equalizer works best for applications whose channel filter transfer function does not have deep amplitude nulls in the distorted signal bandwidth. The DF equalizer works well in channels with deep amplitude nulls; however, there is a possibility of error propagation if an incorrect symbol is used to determine the tap weights. The MLSE is optimal but becomes computationally cumbersome as the ISI trellis length increases.

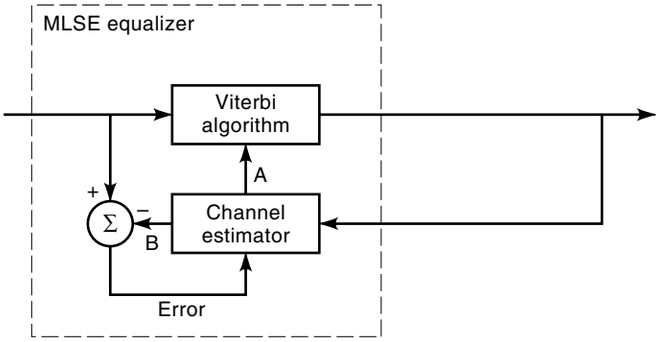

Figure 10. Block diagram of MLSE equalizer used to mitigate channel filtering. A is the channel estimate while B is the received signal estimate. The error signal is used to adjust the channel estimate.

There are several other methods used to mitigate the effects of channel filtering. For example, multipath signals arrive with unique directions of arrival and polarizations; thus the multipath signals can be viewed as sources of direction or polarization diversity. Switched antenna diversity can be used to select an antenna from an array of antennas whose direction or polarization corresponds with the best path (35). Adaptive antenna arrays can be used to form antenna beams that attenuate interfering paths. Multipath signals also arrive with unique time delays. The Rake detector uses direct-sequence signals that have been delayed by the multipath channel as a source of time diversity (36).

Orthogonal frequency-division-multiplexing (OFDM) (37) decreases the effects of ISI by spreading symbols out over longer time periods and inserting guard-time intervals. OFDM symbols begin as coefficients of N evenly spaced carrier frequencies. These carrier-frequency coefficients are spread over N time coefficients via an inverse fast Fourier transform (FFT). A guard interval, equal to the maximum channel time delay, is inserted after each block of time coefficients, and the resulting sequence is transmitted. The receiver removes the guard interval and converts the time coefficients back to frequency coefficients using the FFT.

QUANTIFYING INTERSYMBOL INTERFERENCE EFFECTS

As stated in the introduction, ISI is important because it increases the error ratio of a digital communications radio link. Thus in many radio applications, the effects of ISI are reported in terms of error ratio. The error ratio for band-limiting ISI is computed in the following manner (38). Let the impulse response of the cascaded pulse shape and detection filters be

$$x(t) = p(t) * g(t) \tag{58}$$

Assuming amplitude shift keying, the received signal prior to sampling is

$$v(t) = \sum_{l=-\infty}^{\infty} i_l x(t - lT) + n(t) \tag{59}$$

and the mth sampled symbol is

$$v(mT + \tau) = i_m x(\tau) + \sum_{\substack{l=-\infty \\ l \neq 0}}^{\infty} i_{l+m} x(\tau - lT) + n(mT + \tau) \tag{60}$$

where the first term is the desired symbol value, the second term represents ISI, n represents additive noise, and τ is the sample time offset ranging from 0 to T. The combined probability function, Pr( ), of the noise and ISI is symmetrical about the decision threshold $x(\tau)$; thus

$$P_e = \frac{1}{2} \Pr(|n(\tau) + z(\tau)| \geq |x(\tau)|) \tag{61}$$

where z represents ISI. The difficulty with this approach is that the distribution of z is not generally known; however, bounds have been applied to its behavior and satisfactory results have been obtained. In particular, the error ratio as a function of τ for a fixed SNR was determined for the ideal low-pass pulse, the fourth-order Chebyshev pulse, and the Gaussian pulse. These results showed, for example, that with a symbol sample timing error of $0.1T$, the Chebyshev pulse performed slightly better than the ideal low-pass pulse and the Gaussian pulse performed much better than the ideal low-pass pulse.

The SNR degradation at a fixed error ratio for the two-path, specular multipath channel has been quantified (39). These results show that for binary phase-shift keying, minimal degradation of the SNR at a bit error ratio of 10^{-4} occurs if the second-path time delay is less than $0.1T$ for any value of $|\beta|$ less than 1. Rectangular pulse shaping and symbol sample timing synchronized to the direct ray were used for these results. The error ratio for the GWSSUS channel has been found to be independent of the PDP shape and dependent on the channel root mean square (RMS) delay spread (18,40) of the PDP,

$$\sigma_{\text{RMS}} = \sqrt{\frac{\displaystyle\int_0^{\tau_{\max}} (t - \bar{t})^2 P_h(t)\, dt}{\displaystyle\int_0^{\tau_{\max}} P_h(t)\, dt}} \tag{62}$$

where

$$\bar{t} = \frac{\displaystyle\int_0^{\tau_{\max}} t P_h(t)\, dt}{\displaystyle\int_0^{\tau_{\max}} P_h(t)\, dt} \tag{63}$$

Furthermore simulation studies have shown that the GWSSUS channel has little influence on error ratio if σ_{RMS} is less than $0.1T$. Raised cosine pulses and symbol sample timing synchronized to $\bar{t}$ were used for these results.

CONCLUSION

In this article, the most common ways that ISI is introduced, prevented, and mitigated have been presented. Intersymbol interference will continue to be a problem for radio link engineers because of the proliferation of wireless personal communication devices that operate in frequency-selective multipath channels and the demand for higher-speed data transmission with wider bandwidths. These and other radio applications will continue to motivate engineers to develop new ISI prevention and mitigation techniques.

BIBLIOGRAPHY

1. H. Nyquist, Certain topics in telegraph transmission theory, *Trans. Am. IEE,* **April**: 617–644, 1928.
2. W. R. Bennet and J. R. Davey, Effects of restricted bandwidth, in *Data Transmission,* New York: McGraw-Hill, 1965, pp. 49–77.
3. M. Sablatash, J. L. Lodge, and K. W. Moreland, Theory and methods for design of pulse shapes for broadcast teletext, *IEEE Trans. Broadcast.,* **35**: 40–55, 1989.
4. F. de Jager and C. B. Dekker, Tamed frequency modulation, a novel method to achieve spectrum economy in digital transmission, *IEEE Trans. Commun.,* **26** (5): 534–542, 1978.
5. S. Pasupathy, Nyquist's third criterion, *Proc. IEEE,* **62**: 860–861, 1974.

6. L. E. Franks, Further results on Nyquist's problem in pulse transmission, *IEEE Trans. Commun. Technol.,* **16**: 337–340, 1968.
7. L. E. Franks, Carrier and bit synchronization: A tutorial review, *IEEE Trans. Commu.,* **28**: 1107–1121, 1980.
8. J. J. Jones, Filter distortion and intersymbol interference effects on PSK signals, *IEEE Trans. Commun. Technol.,* **19**: 120–132, 1971.
9. K. Murota and K. Hirade, GMSK modulation for digital mobile radio telephony, *IEEE Trans. Commun.,* **29**: 1044–1050, 1981.
10. J. G. Proakis, Signal design for band-limited channels, in *Digital Communications,* New York: McGraw-Hill, 1995, pp. 534–576.
11. E. S. Sousa and S. Pasupathy, Pulse shape design for teletext data transmission, *IEEE Trans. Commun.,* **31**: 1983, 871–878.
12. S. Youshida and F. Ikegami, A comparison of multipath distortion charactertistics among digital modulation techniques, *IEEE Trans. Veh. Technol.,* **34**: 128–135, 1985.
13. M. C. Jeruchim, P. Balaban, and K. S. Shanmugan, Communication channels and models, in *Simulation of Communication Systems,* New York: Plenum Press, 1992, pp. 362–390.
14. E. D. Sunde, Pulse transmission by AM, FM, and PM in the presence of phase distortion, *Bell Syst. Tech. J.,* **March**: 353–422, 1961.
15. W. D. Rummler, R. P. Coutts, and M. Liniger, Multipath fading channel models for microwave digital radio, *IEEE Commun. Mag.,* **24** (11): 30–42, 1986.
16. D. Parsons, Wideband channel characterization, in *The Mobile Radio Propagation Channel,* London: Pentec Press, 1992, pp. 161–188.
17. P. A. Bello and B. D. Nelin, The effect of frequency selective fading on the binary error probabilities of incoherent and differentially coherent matched filter receivers, *IEEE Trans. Commun. Syst.,* **11**: 170–185, 1963.
18. J. C. I. Chuang, The effects of time delay spread on portable radio communication channels with digital modulation, *IEEE J. Selected Areas Commun.,* **5**: 879–889, 1987.
19. D. C. Cox, Correlation bandwidth and delay spread multipath propagation statistics for 910-MHz Urban mobile radio channels, *IEEE Trans. Commun.,* **23**: 1271–1280, 1975.
20. D. M. J. Devasirvathem, Time delay spread and signal level measurements of 850 MHz radio waves in building environment, *IEEE Trans. Antennas Propagation,* **34**: 1300–1305, 1986.
21. T. S. Rappaport, Small scale multipath measurements, in *Wireless Communications—Principles and Practice,* Upper Saddle River, NJ: Prentice-Hall, 1996, pp. 153–159.
22. J. A. Wepman, J. R. Hoffman, and L. H. Loew, Impulse response measurements in the 1850–1890 MHz band in large outdoor cells, NTIA Report 94-309, June 1994, pp. 3–8.
23. S. Y. Seidel and T. S. Rappaport, A ray tracing technique to predict path loss and delay spread inside building, *Proc. IEEE Golobecom 92,* Orlando, FL, 1992, pp. 649–653.
24. R. A. Valenzuela, A ray tracing approach to predicting indoor wireless transmission, *Proc. IEEE Veh. Technol. Conf.,* Secaucus, NJ, 1993, pp. 214–218.
25. L. Talbi and G. Y. Delisle, Finite difference time domain characterization of indoor radio propagation, in J. A. Kong (ed.), *Electromagnetic Waves Pier 12, Progress in Electromagnetic Research,* Cambridge, MA: EMW Publishing, 1996, pp. 251–275.
26. C. L. Holloway, M. G. Cotton, and P. Mckenna, A model for predicting the power delay profile characteristics inside a room, *IEEE Trans. Vehic. Technol.,* 1999.
27. L. Talbi and G. Delisle, Wideband propagation measurements and modeling at millimeter wave frequencies, *Proc. IEEE Globecom 93,* Houston, TX, 1993, pp. 47–51.
28. A. A. M. Saleh and R. A. Valenzuela, A statistical model for indoor multipath propagation, *IEEE J. Selected Areas Commun.,* **5**: 128–137, 1987.
29. T. S. Rappaport, S. Y. Seidell, and K. Takamizawa, Statistical channel impulse response models for factory and open plan building radio communication design, *IEEE Trans. Commun.,* **39**: 794–807, 1991.
30. H. Hashemi, Impulse response modeling of indoor radio propagation channels, *IEEE J. Selected Areas Commun.,* **11**: 967–978, 1993.
31. C. L. Holloway, M. G. Cotton, and P. McKenna, A simplified model for calculation of the decay rate of the impulse response for an indoor propagation channel, *Proc. 2nd Annu. Wireless Commun. Conf.,* Boulder, CO, 1997, pp. 210–214.
32. P. Chevillat and E. Eleftheriou, Decoding of trellis-encoded signals in the presence of ISI and noise, *IEEE Trans. Communications,* **37**: 669–676, 1989.
33. S. U. H. Qureshi, Adaptive equalization, *Proc. IEEE,* **73**: 1349–1386, 1985.
34. J. G. Proakis and J. H. Miller, An adaptive receiver for digital signaling through channels with intersymbol interference, *IEEE Trans. Inf. Theory,* **15**: 484–497, 1969.
35. T. S. Rappaport, Diversity techniques, in *Wireless Communications—Principles and Practice,* Upper Saddle River, NJ: Prentice-Hall, 1996, pp. 325–335.
36. J. G. Proakis, Communications through band-limited linear filter channels, in *Digital Communications,* New York: McGraw-Hill, 1995, pp. 583–628.
37. W. Y. Zou and Y. Wu, COFDM: An overview, *IEEE Trans. Broadcast.,* **41**: 1–8, 1995.
38. R. Lugannani, Intersymbol interference and probability of error in digital systems, *IEEE Trans. Inf. Theory,* **15**: 682–688, 1969.
39. R. E. Zeimer and W. H. Tranter, Multipath interference, *Principles of Communication: Systems Modulation and Noise,* Boston, MA: Houghton-Mifflin, 1976, pp. 346–356.
40. W. C. Jakes (ed.), *Microwave Mobile Communications,* New York: IEEE Press, 1993.

ROBERT J. ACHATZ
CHRISTOPHER L. HOLLOWAY
Institute for Telecommunication Sciences

SYMMETRY. See DUALITY, MATHEMATICS.

SYNCHRONIZATION, NETWORK. See CLOCKS IN TELECOMMUNICATIONS.